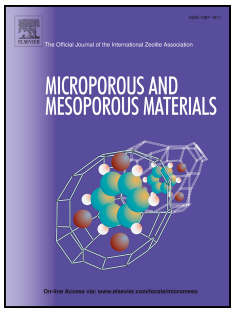

Surface-enhanced CO_2 capture in ionic liquid-silica nanocomposites via sol-gel synthesis in the low partial pressure range

Marieke van Leeuwen, Nina Plankensteiner, Rahul Maity, Jesus Gandara Loe, Joeri F.M. Denayer, Rob Ameloot, Philippe M. Vereecken

PII: S1387-1811(24)00396-2

DOI: https://doi.org/10.1016/j.micromeso.2024.113374

Reference: MICMAT 113374

To appear in: *Microporous and Mesoporous Materials*

Received Date: 21 August 2024

Revised Date: 9 October 2024

Accepted Date: 16 October 2024

Please cite this article as: M.v. Leeuwen, N. Plankensteiner, R. Maity, J.G. Loe, J.F.M. Denayer, R. Ameloot, P.M. Vereecken, Surface-enhanced CO_2 capture in ionic liquid-silica nanocomposites via sol-gel synthesis in the low partial pressure range, *Microporous and Mesoporous Materials*, https://doi.org/10.1016/j.micromeso.2024.113374.

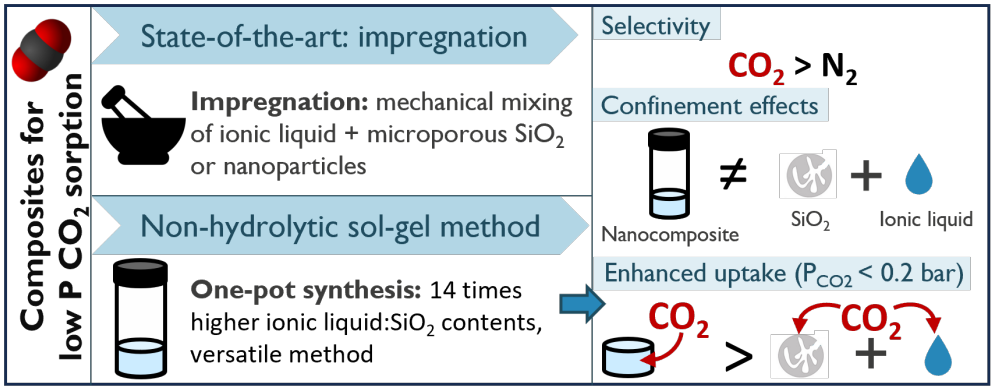

Surface-enhanced CO_2 capture in ionic liquid-silica nanocomposites via sol-gel synthesis in the low partial pressure range

Marieke van Leeuwen[a, b, c], *Nina Plankensteiner*[b, c], *Rahul Maity*[d], *Jesus Gandara Loe*[a], *Joeri F.M. Denayer*[d], *Rob Ameloot*[a], *Philippe M. Vereecken*[b,a,c] *

[a] KU Leuven, Center for Membrane separations, Adsorption, Catalysis & Spectroscopy (cMACS), Celestijnenlaan 200F, 3001 Leuven, Belgium,

[b] imec, Kapeldreef 75, 3001 Leuven, Belgium,

[c] EnergyVille-Thor Park 8320, 3600 Genk, Belgium ,

[d]Department of Chemical Engineering (CHIS), Vrije Universiteit Brussel, Brussels, 1050 Belgium

*Corresponding author: philippe.vereecken@imec.be

ABSTRACT

Ionic liquid-containing silica nanocomposites enable the capture of carbon dioxide from gas mixtures containing nitrogen, oxygen, and methane. Synthesis methods explored for such nanocomposites include impregnating porous silica and one-pot synthesis via a sol-gel process. This research investigates a non-hydrolytic sol-gel route for nanocomposite materials enabling CO_2 capture at low partial pressures (0.1-0.4 bar). The tetraethyl orthosilicate (TEOS) precursor condensation resulted in a silica matrix formed around ionic liquid domains, for bis(trifluorosulfonylimide) ($TFSI^-$)-based ionic liquids with 1-butyl-1-methylpyrrolidinium (BMP^+), 1-butyl-3-methylimidazolium (BMI^+), 1-ethyl-3-methylimidazolium (EMI^+) and 1-hexyl-3-methylimidazolium (HMI^+) cations. Using a one-pot synthesis method enables exploring CO_2 sorption in such nanocomposites for ionic liquid-to-silica contents up to fourteen times higher than in previously reported studies. Moreover, the selected synthesis method provides greater tunability in deposition methods and their control. The silica host matrix was characterized by N_2 adsorption isotherms at 77 K after solvent extraction and supercritical drying of the material for ionic liquid removal. The pore size distribution of the freestanding silica network was observed via Scanning Electron Microscope (SEM) imaging and assessed with the Barrett-Joyner-Halenda (BJH) method for nanocomposites of different [BMP][TFSI]-to-silica ratio. The CO_2 uptake at pressures down to 0.1 bar was evaluated from CO_2 adsorption isotherms at 303 K. The confinement of [BMP][TFSI] resulted in a beneficial effect for the CO_2 uptake at lower partial pressures, with an uptake five times higher than the sum of the individual uptake expected from the contained ionic liquid and silica. The reported results show the advantage of a one-pot synthesis method for broader tunability of the nanocomposite, both regarding its content and application, as well as increased performance at lower partial pressures compared to the nanocomposite's individual constituents.

INTRODUCTION

The increase in anthropogenic greenhouse gas emissions since the Industrial Revolution has deleteriously impacted the climate on Earth [1]. In order to limit the global temperature rise to +1.5°C by 2100 with respect to pre-industrial times, only 6 years of CO_2 emissions at the current rate of release are permitted [2]. Containment policies such as CO_2 capture strategies are already considered necessary as per the latest Intergovernmental Panel on Climate Change (IPCC) report [3]. CO_2 capture can be carried out at different stages, *e.g,* directly from the air or more concentrated sources like flue gases.

Both absorption and adsorption processes using solvents or porous solid materials have been explored for post-combustion CO_2 capture from flue gas-like streams. The latter are the products of industrial combustion processes, which are typically composed of *ca.* 70% of N_2, 10-15% CO_2, 5-10% H_2O and 10% O_2, and emitted at pressures around atmospheric conditions [4], [5]. The most mature technology available for industrial CO_2 scrubbing relies on absorption in amine-based solvents, *e.g.*, monoethanolamine in water [6]. The uptake mechanism is based on the chemical reaction of CO_2 and an amine group to form carbamate salts. Though the reaction kinetics are fast and thus opportune for CO_2 capture (especially for primary amines), the enthalpy of the reaction has to be overcome for solvent regeneration and therefore requires high energetic efforts. Other drawbacks of this process include the volatility and corrosiveness of the sorbent, as well as its degradation with oxygen [4].

Ionic liquids (IL) offer a versatile alternative as physical and chemical sorption media for carbon dioxide capture. In 1999, Blanchard et al. first reported significant CO_2 solubility properties in 1-butyl-3-methyl imidazolium hexafluorophosphate ([BMI][PF_6]), opening the field to CO_2 capture using ionic liquids [7]. Bulk ionic liquids have gained tremendous interest over the past century, growing exponentially from a handful of yearly research papers to over 7000 research papers in 2024 [8]. They indeed have negligible vapor pressure, high thermal stability with decomposition temperatures ranging from 200-430 ºC, and are typically non-flammable [9]. Their composition is easily tuned to application needs and is highly recyclable. Upon careful selection, high CO_2 uptake capacity and selectivity over main flue gas components, such as N_2, can be achieved, making them promising competitors to the aforementioned amine-based solvents. The use of physical ionic liquids for CO_2 capture and sequestration allows an important decrease of energy consumption and energy required for regeneration (15 to 40% less compared to typical amine-based solvents) [10]. Moreover, capture in physical ionic liquids allows faster kinetics than capture via chemisorption.

Physical ionic liquids used for CO_2 capture via physisorption are typically composed of bulky ions with, among others, fluorinated or alkylated groups. These molecules are highly complex as the charge distribution across the molecule can vary depending on the counter ion or the surrounding of the ionic liquid itself. Therefore, unraveling the underlying physisorption mechanisms is not straightforward. Physisorption in bulk ionic liquids is most likely a result of combined effects, including Lewis acid-base interactions between the anion and the sorbate [11],

[12]. However, this is not the only mechanism involved, as the carbon dioxide uptake does not always follow the basicity order when varying the anion, as was reported for [BMI][BF_4] and [BMI][PF_6] [11]. Fluorination of both the anion and cation has been reported to result in some "CO_2-philic" properties of ionic liquids, though the evidence itself and the mechanisms for this phenomenon are debated [13]. The role played by the free volume of the ionic liquid, defined as the molar volume corrected for the van der Waals molar volume, seems to be the most reliably reported trend. It indeed holds for a wide range of ionic liquids, as supported by computational and experimental studies. Increasing cation alkyl chain length positively enhances the presence of such a free volume and has been reported to yield higher CO_2 solubility [14]. Even though ionic liquids showcase some promising features as CO_2 capture media, their performance as physical absorbents is most relevant in the high CO_2 partial pressure range.

Several strategies, including amine functionalization [4], have been reported to increase the performance of ionic liquids for CO_2 sorption at low partial pressures, as required for the low CO_2 concentration in flue gas streams. Carboxylate functionalized anions, *e.g.* [bmim][acetate] have properties intermediate to MEA and physical ILs. The volumetric absorption capacity for an acetate-based ionic liquid is *ca.* 25m^3/m^3, which is intermediate to 65m^3/m^3 for MEA and 3m^3/m^3 for physical ionic liquids. Their enthalpy of reaction (−40kJ/mol) is comprised between that of MEA (−85kJ/mol) and physical ILs (−15kJ/mol) [4]. Alternative methods to increase the performance while keeping the regeneration energy relatively low include the confinement of an ionic liquid on a host matrix, *e.g.,* formed of silica [15], [16], [17].

The fabrication of ionic liquid-silica composites for CO_2 capture has most commonly been implemented by immobilizing the ionic liquid in porous silica particles via impregnation methods (Table 1). Pre-synthesized or commercial silica particles are mechanically mixed with an ionic liquid, until a gel is obtained. Two parameters can notably be varied: the pore size of the host matrix, and the ionic liquid fraction loaded into the pores. Some limitations of the process include a tedious mixing step, as well as a physical limitation of the amount of ionic liquid in the pores, as exemplified by the maximum final IL:SiO_2 reported so far in literature for CO_2 uptake from ionic liquid-silica composites (Table 1). Sol-gel reaction pathways offer an elegant alternative to the impregnation process, as the material can be synthesized in a one-pot reaction step. The sol synthesized before gelation offers a larger variability in material composition and new opportunities for material integration for different applications. In the sol-gel process, the hydrolysis and condensation reactions of, for example, a tetraethylorthosilicate (TEOS) precursor as used in this study, occur in-situ, resulting in the formation of a thin, high surface area silica matrix built around ionic liquid domains. The versatile material fabrication methods include thin layer coatings on substrates via spin-coating or drop-casting or even conformal coatings on 3D materials via dip-coating. Though some promising uptake capacities were previously achieved, with 5 studies exceeding 1 mmol/g maximum uptake via the impregnation method, most feed streams considered were atmospheric or pressurized carbon dioxide streams. Flue gas streams are a major source of CO_2 emissions, and their emission conditions are typically at much lower CO_2 partial pressures (0.1 - 0.15 bar) [4].

This work explores the confinement of ionic liquids in a silica host matrix via a non-hydrolytic sol-gel synthesis route for enhanced CO_2 sorption at low partial pressures. Bis(trifluorosulfonyl)imide ([$TFSI^-$])-based ionic liquids with imidazolium and pyrrolidinium cations were selected for confinement due to their low CO_2 solubility in bulk form compared to other physical ILs [18], [19], [20], [21]. Via this synthesis procedure, high ionic liquid content composites (up to 2 mol IL:mol TEOS) were prepared and studied for the first time as CO_2 sorbent materials in the low partial pressure range (0.1-0.4 bar). A confinement effect was observed in this pressure range, yielding a CO_2 uptake higher for the composite material than for the sum of its components.

Table 1. Ionic liquid-silica composites reported in the literature for CO_2 sorbent synthesized via impregnation and sol-gel synthesis methods. Ionic liquids cations reported are 1-ethyl-3-methylimidazolium ([EMI^+]), 1-butyl-3-methylimidazolium ([BMI^+]), 1-propyl-3-methyl imidazolium ([PMI^+]), 1-octyl-3-methylimidazolium ([OMI^+]), tetrabutylphosphonium ([$P4444^+$]), tetrahexylammonium ([N6666]), N,N,N-trimethyl-N-ethylammonium ([4TE]), and 1-ethylamine-3-methylimidazolium (AmMI). Anions reported were NO_3^-, SCN^-, $N(CN)_2^-$, $HSO4^-$, bis(trifluorosulfonyl)imide ([$TFSI^-$]), acetate, prolinate ([Pro]), Br^-, 2-hydroxypyridine ([2-Op]), BF_4. Maximum uptake reported at [a]25°C, [b]30°C, [c]40°C, [d]45°C, [e]50°C.

Average pore size [nm]	ILs	Max. final IL:SiO_2 wt	Maximum CO_2 uptake [mmol/g]	P range [bar]	Reference
Gel from mesoporous silica via impregnation					
3.5	[BMI][NO_3] [BMI][SCN] [BMI][$N(CN)_2$]] [BMI][HSO_4]	1:1	0.35[a] 0.28[a] 0.30[a] 0.53[a]	1	[22]
1	[EMI][TFSI] [OMI][TFSI]	1:1	0.5[c] 0.9[c]	0.1-2.5	[23]
3	[BMI][Acetate] [PMI][TFSI]	0.6:1	1.16[b] 0.2[b]	0.1-10	[24]
11*	[BMI][Acetate] [PMI][TFSI]	0.6:1	0.89[b] 0.2[b]	0.1-10	[24]
2.7	[MBMI][TFSI] [MBMI][Br]	0.3:1	1.25[d] 1.86[d]	4-23	[25]
13.5	[P4444][2-Op]	0.15:1	1.68[b]	1	[26]
11	[P4444][2-Op]	0.3:1	1.69[e]	0.1-0.2	[27]
6	[N6666][Pro]	0.4:1	0.36[a]	1	[28]
6	[AmMI][BF_4]	0.55:1	1.61[a]	1	[29]
Gel from dense silica nanoparticles					
20-30**	[4TE][Pro]/H_2O	0.4:1	1.47[c]	1	[30]
Sol-gel process					
3-12	[OMI][BF_4]	0.4	0.082[b]	1	[16]

* *Retrieved for SBA-15 from* [31]

***Particle size*

EXPERIMENTAL SECTION

1. MATERIALS

Tetraethyl orthosilicate (TEOS, 99 %, 86578), formic acid (97.5-98.5 %, F0507) and 1-butyl-3-methyl imidazolium bis(trifluoromethylsulfonyl)imide ([BMI][TFSI], 98 %, 490092) were purchased from Sigma Aldrich. The 1-butyl-1-methylpyrrolidinium bis(trifluoromethylsulfonyl) imide ([BMP][TFSI], 99.9 %) and 1-ethyl-3methylimidazolium bis(trifluoro methylsulfonyl)imide ([EMI][TFSI]) were obtained from Solvionic S.A., and the 1-hexyl-3-methylimidazolium bis(trifluoromethylsulfonyl)imide ([HMI][TFSI], 99%) from Ionic Liquids Technologies GmbH.

2. SYNTHESIS METHODS

2.1. NON-HYDROLYTIC SOL-GEL ROUTE

TEOS/ HCOOH/ IL in molar ratios 1/7.8/x were used, with x values of 0.5, 1, 1.5, and 2. The ionic liquid and formic acid were stirred prior to the addition of the solution to a sample vial containing the TEOS. The total solution volume was kept at 3 mL for all samples. After mixing the components, sample vials were closed and kept at 25 °C in a temperature and humidity-controlled chamber (SH-641, ESPEC Corp.) for 7 days, and gelation typically occurred within 90 min. The gelated samples were dried at a reduced pressure of 80kPa for 7 days at room temperature and subsequently for 12 h under vacuum at 25 °C. The drying process was monitored by weighing with a semi-micro balance (SM 1245Di-C, VWR). A single pellet was obtained for each sample vial.

2.2.THIN FILM COATINGS

Coatings of silica-[BMP][TFSI] composites onto substrates were prepared for different material analyses. The mixed precursor of the non-hydrolytic sol-gel route described above, with the addition of a HCOOH/[BMP][TFSI] mixture to TEOS in a 1/7.8/x TEOS/HCOOH/[BMPTFSI] molar ratio, was drop-casted onto the substrates without ageing, and the samples were dried on a hotplate at 120°C for 1h. Unless otherwise specified, the samples for Raman analysis were deposited at thicknesses of approximately 75µm on silicon wafers. Sol volumes of 53, 46, 42 and 40µL were dropcasted onto 2x2cm wafers for x = 0.5, 1, 1.5 and 2, respectively.

3. MATERIAL CHARACTERIZATION METHODS

Thermo-Gravimetric Analysis (TGA) was performed using a TA Instruments 5500 Discovery under 25 NmL/min N_2 flow at a heating rate of 1 °C/min.

Raman Spectroscopy was performed using a Renishaw VirsaSystem for Raman spectral analysis using visible excitation at 532 nm and VRP20C-532 confocal fiber-optic probe. A 50x objective was used to focus the laser beam on the sample surface. Measurements were done at a laser power

of 5 mW, 50 s exposure time and 3 accumulations in the 100-4000cm^{-1} range. To study the confinement effect by assessing the Raman signal peak shift, a Horiba Jobin-Yvon HR800 instrument for Raman spectral analysis using visible excitation at 785 nm with 100% Neutral Density (ND) filter, 1000 µm confocal hole, 1800 grooves/mm grating was employed. A 10X Olympus objective was used to focus the laser light on the sample surface, and a double exposure of 2*50 s with spike filter to eliminate cosmic spikes was implemented. The spectral resolution, approximated as the interval between two measured datapoints, amounted to ~0.15 cm^{-1}. To study the peak position of the [TFSI$^-$] "breathing" mode, the signals obtained were smoothed using the Origin 75 % percentile filter to reduce the effect of localized noise. A median value of a group of surrounding points is thereby taken for each raw data point.

Shifts in phase transitions upon confinement of the ionic liquid in the nanocomposites were assessed using Differential Scanning Calorimetry (DSC) on a DSC-Q2000 from TA instruments. The standard procedure consisted of a heating step to erase thermal history at a ramp rate of 10 ºC/min until

0 ºC, followed by a cooling step at 5 ºC/min from 200 to -70 ºC, and subsequent heating to 200 ºC at a ramp rate of 1 ºC/min. A sample amount of approximately 10 mg was loaded into a hermetically sealed aluminum pan in a glove box to avoid interferences caused by water uptake of the nanocomposites. The pans were punched upon loading and kept under 50 mL/min N_2 flow during the measurement. An empty pan was used as reference. The reported heat flow was normalized to the loaded sample mass.

The silica matrix's porosity was assessed after the removal of the ionic liquid from the composites via solvent extraction and subsequent CO_2 supercritical drying. The sample was soaked in ethanol for 36 h before the critical point drying procedure started. An Automegasamdri-916B instrument was used to perform the supercritical drying. The temperature was first decreased to 8 °C. The chamber was then filled with CO_2, increasing the pressure to 800 psi, and subsequently purged for 20 min. The chamber pressure was then increased to 1500 psi at 40 °C and maintained for 5 min. Bleeding was finally performed over a time span of 10 min.

The material morphology of the silica-ionic liquid composites after extraction of the ionic liquid was characterized with a Thermo Fisher Verios 5 XHR Scanning Electron Microscope (SEM) with acceleration voltage of 3 kV and current of 25 pA at a working distance of 2.4 mm, using a TLD detector. N_2 adsorption isotherms at 77 K were performed on a Micromeritics 3Flex physisorption instrument to determine the pore size distribution after drying at 100 °C under vacuum for 12 h.. The Barrett-Joyner-Halenda (BJH) method was used on the desorption branch to determine the average pore size and pore volume and was obtained directly from the Flex software from

Micromeritics and cross-checked using the method described in SI S.1.2. The Brunauer-Emmett-Teller (BET) surface area was determined using the Flex software from Micromeritics.

An Autosorb 1 (Quantachrome Instruments, Odelzhausen, Germany) was used to measure CO_2 sorption isotherms for ionic liquid-silica composites at 303 K. Prior to the measurement sample drying was carried out at 100 °C under vacuum for 12 h.

Dynamic breakthrough experiments were performed on a custom-built set-up. A 10 cm length and 1cm inner diameter column was packed with 5.441 g of sorbent and kept in a temperature chamber. Activation was done for 10 hours under helium flow at 100 °C. The breakthrough experiment was performed at 25 °C and 1 bar, with a total flow of 20 NmL/min (50 CO_2:50 N_2), controlled with Bronkhorst thermal mass flow controllers. The column outlet was diluted with 20 NmL/min of helium and directed to a mass spectrometer (MS) to measure the respective concentrations from the column. A detailed description of the method has been provided previously and can be referred to if needed [32]. The amount adsorbed q_a was calculated based on F, the total flow rate, τ_a the mean residence time, ϵ the adsorbent column porosity, V the column volume, m_{ads} the mass of the adsorbent, P the pressure inside the column, x_a the mole fraction of a in the gas phase, R the universal gas constant and T the column temperature (Equations (1) and (2)).

$$q_a = \frac{\left(F\tau_a - \frac{\epsilon VP}{RT}\right) * X_a}{m_{ads}} \quad (1)$$

$$\tau_a = \int_0^\infty (1 - F_{outlet}/F_{inlet})\, dt \quad (2)$$

RESULTS AND DISCUSSION

1. MATERIAL CHARACTERIZATION

The high versatility of the sol-gel process described in this work enables to deposit the material in different forms, *e.g.,* centimeter thick pellets and thin film coatings. Not only does this widen the range of applications, it also opens the door to a broader range of characterization techniques. While pellets offer an adequate support for bulk material properties' studies, including composition from thermogravimetric analysis and CO_2 uptake from adsorption isotherms, coatings offer a controlled platform for spectroscopy studies.

1.1. THERMOGRAVIMETRIC ANALYSIS

The actual ionic liquid-to-silica ratio in the synthesized nanocomposites was evaluated using Thermo-Gravimetric Analysis (TGA). The materials synthesized as defined in the experimental methods consist, after drying, only of ionic liquid and silica, therefore the sum of their share will amount to 100 %. As exemplified in Figure 1, pure [BMP][TFSI] starts to decompose around 250 °C until 470 °C. The SiO_2 fraction, on the other hand, remains at temperatures up to 700 °C. To

minimize the water uptake effect on total mass of the nanocomposite, samples were kept in a glove box after drying and loaded directly in the instrument. The silica content for all samples was normalized to the remaining mass after water evaporation. The measured silica mass percent ranges from 18, 9.9, 7.2, and 6.0 wt.% SiO_2 for x = 0.5, 1, 1.5 and 2 mol ionic liquid: mol TEOS, respectively, and is thereby in a similar range as the expected content from synthesis (22, 13, 8.7 and 6.7 %, respectively). The remaining shares correspond to the mass percent ionic liquid in the sample.

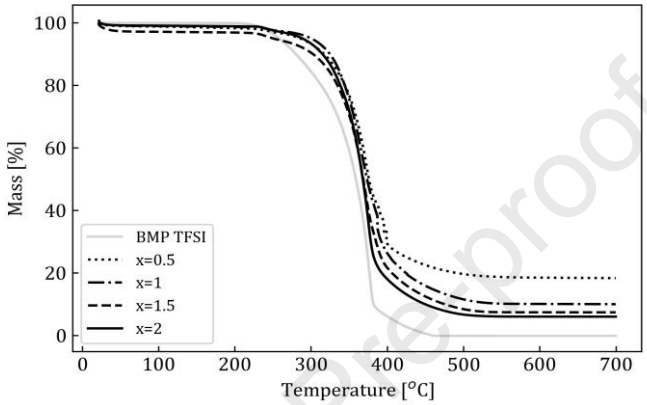

Figure 1. TGA curves of pure [BMP][TFSI] (light grey), and nanocomposite materials with [BMP][TFSI]-to-SiO_2 molar ratios 0.5 (··), 1 (−·), 1.5 (——) and 2 (-), measured under N_2 flow. The SiO_2 content can be read as the plateau value at 700 °C, and was normalized to the remaining mass after water evaporation at 100 °C.

1.2. PORE SIZE DISTRIBUTION OF THE SiO_2 MATRIX

The structure of the inorganic host matrix has an important impact on the arrangement of ionic liquid ion pairs confined in the network and their availability for CO_2 capture [26]. The interconnection of pores is important to ensure a pathway for the diffusion of CO_2 through the material and, therefore, maximal availability of adsorption sites. Moreover, the pore sizes of the SiO_2 network are expected to play a major role in the ionic liquid configuration. For impregnated silica particles, both pore size and pore filling ratio affect the ion-wall interactions and molar volume of the organic filler [15], [33]. These heterogeneous interfacial interactions can enhance the CO_2 uptake in confined sorbent materials [17], [34].

The ionic liquid ([BMP][TSFI]) was extracted from the silica matrix via solvent extraction and CO_2 supercritical drying to prevent pore collapse upon extraction [35]. The preservation of the pore structure after extraction is shown using a Scanning Electron Microscope (SEM) (Figure 2). A lung-like structure can be observed in Figure 2a, with larger pores, similar to bronchioles, providing a pathway towards many smaller pores where gas can be stored, similar to alveoli. These smaller domains result in a high surface area of the host matrix, and, when filled with ionic liquid,

will enable high CO_2 retention, while the bronchioles-like domains ensure accessibility, as visible in the higher magnification SEM image (Figure 2b).

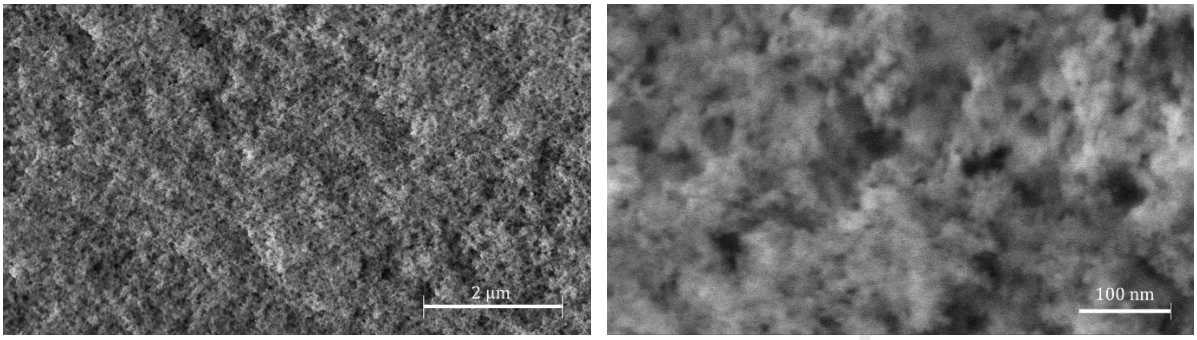

(a) Magnification 15000 (b) Magnification 200000

Figure 2. SEM image of the silica matrix after [BMP][TFSI] extraction via CO_2 supercritical drying for x = 2 mol [BMP][TFSI]: mol SiO_2 under (a) 15000x and (b) 200000x magnification.

The N_2 adsorption/desorption profiles at 77 K in Fig. 3(a) are characteristic of an entirely mesoporous silica matrix and a meso/microporous material for composites synthesized with x = 1 and x = 2 mol [BMP][TFSI]: mol SiO_2, respectively. The small extent of open hysteresis in the adsorption/desorption profiles strongly suggests a well ordered porosity and a connected porous network. The different microstructures observed for nanocomposites of composition x = 2 supports the observations from SEM that two domains are present for x = 2, highlighting the presence of larger "distribution" canals interconnected with smaller pores. Surface area and average pore diameter for the remaining silica after [BMP][TFSI] extraction of the nanocomposites were quantified from the sorption isotherms at 77 K (Fig. 3a) via the Brunauer-Emmett-Teller (BET) and Barrett-Joyner-Halenda (BJH) method. The respective BET surface area amounted to 169 and 293 m^2/g for x = 1 and x = 2 mol IL: mol SiO_2, and the average pore width based on the BJH desorption branch was 14 and 24 nm (Table 2). For smaller ionic liquid-to-silica content, *i.e.,* for $x = 1$, most of the pore volume can be accounted for by pores ranging from 5 to 10 nm radius, as shown in black in the pore size distribution derived from the BJH analysis (Figure 3b). For higher ionic liquid content, *i.e.*, for $x = 2$, some domains can be differentiated. Pores of radius around 20 and 40 nm account for a large volume fraction of the silica host matrix, as visible from the wide distribution in Figure 3b, and can be related to the bronchiole's highways observed in Figure 2. Smaller domains inferior to 10 nm are also found and can be related to the smaller alveoli. The sol-gel synthesis route created an interconnected porous silica network with high ionic liquid retention, thereby standing out from previous ionogel compositions in CO_2 sorption studies (Table 1). The total pore volume amounts 0.63 cm^3/g and 0.88 cm^3/g for the $x = 1$ and $x = 2$ extracted nanocomposites, as calculated from the BJH method from the isotherms presented in Fig.3a (see methods and SI). This translates to 59 and 66 vol %, respectively, using a density for amorphous silica of 2.2 g/cm^3 [36].

Table 2. Parameters obtained from N_2 isotherms at 77 K for the silica host matrix for composites with [BMP][TFSI]-to-SiO_2 molar ratios of x=1 and x=2 after [BMP][TFSI] removal via solvent extraction.

	x=1	x=2
Surface area [m^2/g]	169	293
Average pore width [nm]	14	24
Total pore volume [cm^3/g]	0.63	0.88
Pore volume [%]	59	66

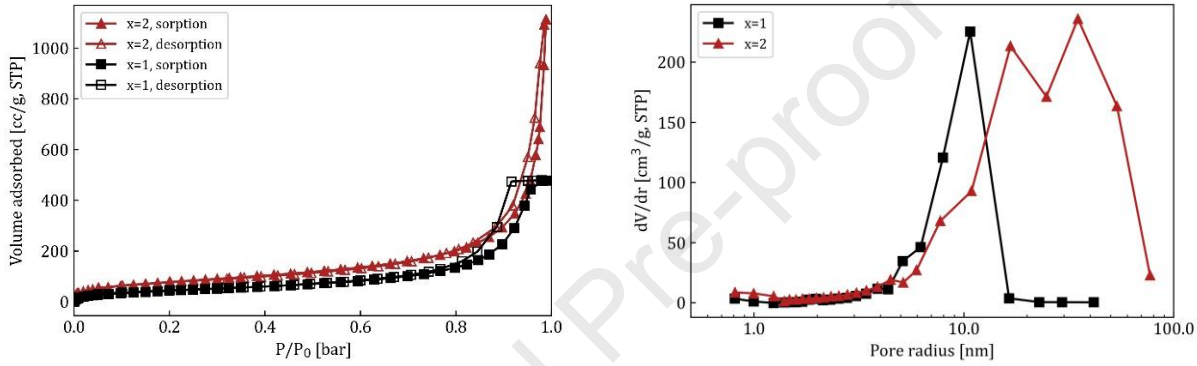

(a) (b)

Figure 3: (a) N_2 adsorption/desorption measurements at 77 K of mesoporous silica after the extraction of [BMP][TFSI] from the composite materials for x = 1 and x = 2 mol [BMP][TFSI]: mol SiO_2 contents. (b) Pore size distribution analysis derived from the BJH method using the desorption branch of the N_2 isotherm at 77 K assuming rigid cylindrical pores and contact angle of 0°, for the silica host matrix of composites with [BMP][TFSI]-to-SiO_2 molar ratios of x=1 and x=2 after [BMP][TFSI] removal.

1.3. [$TFSI^-$] ANION CONFORMATION UPON IONIC LIQUID CONFINEMENT IN SILICA

Raman spectroscopy confirmed the presence of the expected individual components of the nanocomposite material in both pellets and coatings, showing typical Raman signatures for the [BMP][TFSI] cation and anion, as well as the silica host matrix (see supplementary information, Figure S5). The 200-1000 cm^{-1} range of the Raman spectrum provides more insight into the conformation and confinement of the [$TFSI^-$] anion in the silica host matrix, which is known to play a significant role in CO_2 sorption in ionic liquids [4]. Typical Raman peaks for the [$TFSI^-$] anion were identified for all *x* values studied and are presented in Figure 4.

The lower wave numbers (marked in blue in the figure) represent the rocking modes (ρ) of the anion's CF_3 terminations and SO_2 groups [37]. The [$TFSI^-$] anion can be found as two different conformers, namely the cis (C_1) and trans (C_2) configurations. Insights on the ratio of both conformers can be obtained in the 260-360 cm^{-1} region. In the latter, five distinct bands were observed at 279, 298, 315, 327, and 341 cm^{-1}, with the first, second, third, and fifth attributed to the C_2 configuration [38], [39], [40] and the fourth to the C_1 conformer [38], [40], [41]. The rocking of the CF_3 band is more pronounced in the trans (C_2) conformation due to the molecule geometry, resulting in these four peaks. The first peak is intensified by the additional dipole moment change caused by the rocking of the SO_2 group, which also has more vibrational freedom in the C_2 than in the C_1 conformer. For the silica-ionic liquid nanocomposites, the intensity of the 279 cm^{-1} peak relative to the four other [$TFSI^-$] peaks decreases compared to the bulk ionic liquid. The C_2 conformer might, therefore, be relatively less represented than for the bulk [BMP][TFSI], in line with the findings of Garaga et al. for the confinement of ionic liquid in nanoporous silica microparticles [33]. The SC stretching vibrational mode expected at 327 cm^{-1} is nearly inactive for the trans-conformer due to symmetry constraints of the conformation, whereas a clear peak appears for the cis-[$TFSI^-$] conformer [38].

In the 580 to 600 cm^{-1} region, the bending (δ) modes for the SNS bond at the center of the anion, its CF_3 terminations and the SO_2 bonds can be found. An intense characteristic band for the [$TFSI^-$] anion is found around 742 cm^{-1}. The latter corresponds to an "expansion-contraction" mode of the ion, sometimes referred to as a "breathing mode". This band is attributed to the complex collective motion of atoms in the anion, more specifically to the bending modes of SO_2 and CF_3 coupled with the bending and stretching vibrations of the SNS bond [38], [42], [43].

When decreasing the IL-to-SiO_2 molar ratio from $x = 2$ to 0.5, a shift in peak position for the [$TFSI^-$] "breathing mode" was observed towards lower frequencies, as shown in Figure 5. For $x = 2$, the peak is found at the same position as for bulk [BMP][TFSI], while for $x = 0.5$, the peak appears around 1 cm^{-1} lower.

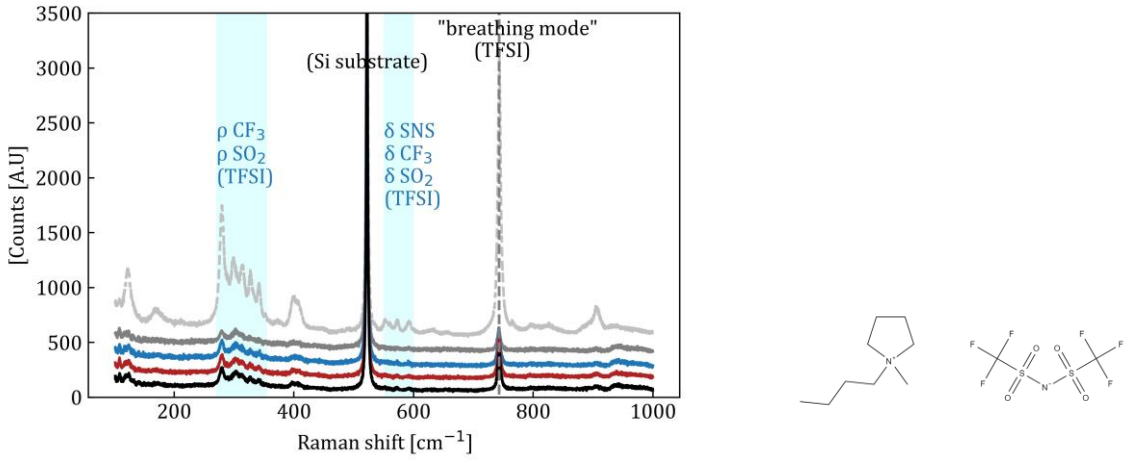

(a) (b)

Figure 4. (a) Raman spectrum of the pure [BMP][TFSI] ionic liquid (light grey dotted) *vs.* [BMP][TFSI] confined in silica via a solvolytic sol-gel method, with x = 0.5 (grey), 1 (blue), 1.5 (red) and 2 (black), defined as the molar ratio between ionic liquid and silica precursor x = (mol IL:mol SiO_2) in the 200-1000 cm^{-1} range. (b) Molecular structure for [BMP][TFSI].

The [$TFSI^-$] "breathing mode" of the C_2 conformer has been reported around 742 cm^{-1} from computational studies, against 739 cm^{-1} for the C_1 configuration [38], [44]. Thus, the shift could be attributed to a preferred C_1 cisoid orientation upon increasing the silica content of the nanocomposite. This shift could, however, also be attributed to a loss of vibrational freedom of the [$TFSI^-$] anion as a result of the interaction with the neighboring silica wall without necessarily hinting at a preferred conformation.

Overall, the surroundings of the ionic liquid are bound to impact its physicochemical behavior compared to the bulk state. The smaller average pore size of the nanocomposites with x=1 compared to x=2 results in a relative larger fraction of [BMP][TFSI] experiencing interactions with the silica wall (interface region) compared to the fraction of the ionic liquid in the core of the pore (bulk region). Similar effects have previously been reported for ionic conductivity enhancement in IL-SiO_2 nanocomposites electrolytes [45]. Ionic liquid confinement effects for lower [BMP][TFSI]-to-silica contents were further evidenced by a decrease in melting temperature observed from DSC for nanocomposites with lower ionic liquid-to-silica contents (Fig. S6). The shift towards lower melting temperatures for more confined [BMP][TFSI] is attributed to a decrease in ionic liquid-pair interactions due to more dominant interactions between the ionic liquid and silica termination (-OH), in line with the spectroscopic observations.

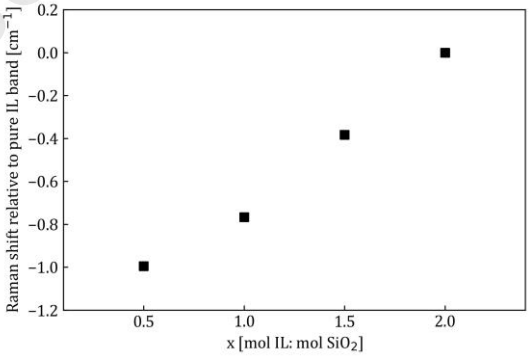

Figure 5. Relative Raman shift with respect to the [$TFSI^-$] "breathing" mode in pure [BMP][TFSI] (742 cm^{-1}) for different silica-ionic liquid nanocomposites synthesized via non-hydrolytic method with x the molar ratio of [BMP][TFSI]-to-SiO_2 precursor.

2. CO_2 ADSORPTION PERFORMANCE CHARACTERISTIC OF THE IL-SILICA NANOCOMPOSITES

2.1. CO_2 UPTAKE FOR [BMP][TFSI]-SIO_2 NANOCOMPOSITES

2.1.1. GENERAL ADSORPTION TRENDS, REVERSIBILITY, AND EXCLUSION OF DIFFUSION EFFECTS

CO_2 adsorption isotherms were measured to compare the CO_2 uptake capacity of the different synthesized nanocomposites. A maximum uptake was reached around 0.13 mmol/g for x=0.5 and 2 mol [BMP][TFSI]: mol SiO_2 at 303 K and 1 bar, 0.12 mmol/g for x=1 and 0.10 mmol/g for x=1.5. This value is in the lower range compared to the state-of-the-art for impregnated ionic liquid-silica composites (cf. Table 1), and surpasses the uptake for a previous sol-gel method reported for CO_2 sorption (0.082 mmol/g at 1 bar, 303 K [16]). As a general trend, a sharper increase in CO_2 uptake with increasing partial pressure was observed in the lower pressure range, as exemplified in Figure 6a for a nanocomposite with different [BMP][TFSI]-to-silica molar ratio. All four nanocomposites presented similar CO_2 adsorption isotherms, suggesting that the absolute ionic liquid content immobilized was not a key parameter influencing CO_2 uptake.

A small hysteresis was observed on the desorption branch. For most isotherms, a 5 min equilibration time (in red in Figure 6b) was given at each pressure. Given the typically slow diffusion of CO_2 through the nanocomposites, longer equilibration times of 60 min (black) were tested to cross-check and exclude diffusion effects as reported in other studies for impregnated silica particles [23]. The equilibration time did not affect the measured uptake on the sorption branch for the three duplicated pressures. The difference seen between 5 and 60 min equilibration time falls within the experimental error range (cf. fig. S1). The hysteresis disappeared for desorption with longer equilibration times, showing that given enough time, the material could release all the sorbed CO_2.

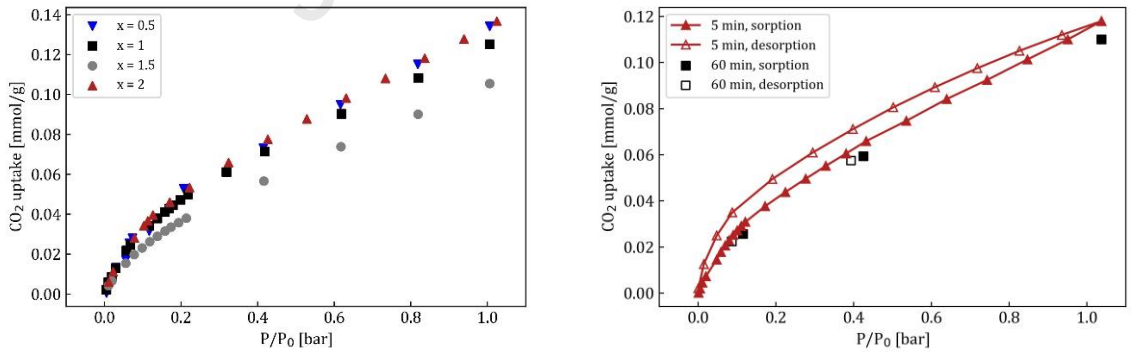

(a) (b)

Figure 6. (a) Average CO_2 adsorption measurements at 303 K for 1-butyl-1-methylpyrrolidinium bis(trifluoromethylsulfonyl)imide ([BMP][TFSI])-SiO_2 composite with molar ratio x ranging from 0.5 to 2. (b) CO_2 adsorption/desorption measurements at 303 K of a [BMP][TFSI]-SiO_2

nanocomposite with molar ratio x = 2 given 5 (red, triangle) or 60 min (black, square) threshold equilibration time.

2.1.2. DYNAMIC BREAKTHROUGH EXPERIMENTS FOR COMPETITIVE CO_2/N_2 SORPTION

TFSI-based ionic liquids are suitable candidates for CO_2 sorption from flue gases due to their high selectivity for CO_2 compared to other gases such as N_2, whereas SiO_2 does not offer this selectivity. Ionic liquid-silica composites have been demonstrated to keep the ionic liquid selectivity characteristics [23]. A breakthrough experiment at 298 K was performed using a gas mixture containing 50 vol% CO_2 in N_2 to confirm the selectivity also for the sol-gel synthesized [BMP][TFSI]-silica nanocomposites. Figure 7 shows that N_2 is nearly immediately breaking through the column upon passing a mixed N_2-CO_2 feed over a column packed with a[BMP][TFSI]-SiO_2 nanocomposite of molar ratio x = 1, confirming the very low affinity for N_2. CO_2 is breaking through the column about half a minute later (red). The total accumulation of the sorbates amounted 0.053 mmol/g and 0.0099 mmol/g for CO_2 and N_2, respectively. From the adsorption isotherms, an average CO_2 uptake of 0.077±0.02 mmol/g at 0.5 bar CO_2 and 303 K was determined for two nanocomposites with same composition of x = 1. Hence, considering the spread in uptake and the presence of a temperature effect in the breakthrough experiment due to the exothermicity of CO_2 adsorption, both methods yielded a similar result in capacity.

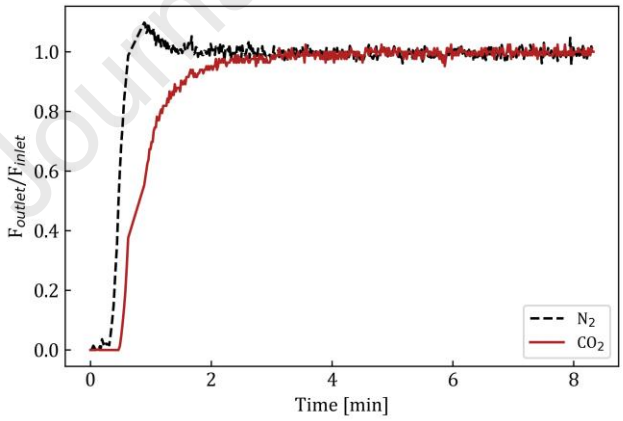

Figure 7. The adsorption branche of the breakthrough experiment showing the ratio of outlet flow over inlet one for both CO_2 and N_2 with time for a 1-butyl-1-methylpyrrolidinium bis(trifluoromethylsulfonyl)imide ([BMP][TFSI])-SiO_2 nanocomposite with molar ratio x = 1 with a gas feed of composition of 50% CO_2: 50% N_2 at 298 K.

2.2. INTERFACIAL EFFECTS FOR ENHANCED CO_2 SORPTION

2.2.1. ENHANCEMENT EFFECT FOR CO_2 CAPACITY IN [BMP][TFSI]-SILICA NANOCOMPOSITES

Confinement effects of the [BMP][TFSI] ionic liquid in a silica matrix were found to positively influence the CO_2 uptake, especially at lower partial pressures and higher ionic liquid-to-host matrix ratios. Nanocomposites of x = 0.5, 1, 1.5 and 2 mol IL:mol SiO_2 were synthesized in pellet form as described in the experimental section. The CO_2 uptake was evaluated from adsorption isotherms at 303 K (Fig. 6). The uptake for the x = 2 nanocomposites at different partial pressures, is presented in black in Figure 8. The CO_2 uptake capacity was found to be around 0.03 mmol/g nanocomposite at 0.1 bar and around 0.125 mmol/g at 1 bar. As a result of the isotherm non-linearity, the uptake at 0.1 bar is approximately four times lower than at 1 bar. A breakdown of expected uptake was added to assess the performance of the nanocomposite material with respect to its individual components, namely SiO_2 and [BMP][TFSI]. Firstly, in region (1), the uptake for pure SiO_2 is plotted, as the uptake per unit surface area normalized to the SiO_2 weight fraction in the nanocomposite. Secondly, in region (2), the normalized expected uptake of [BMP][TFSI] is shown, based on the reported uptake for the pure ionic liquid at different partial pressures [18]. An uptake enhancement (3) is identified as the difference between the nanocomposite uptake and the sum of the expected uptake for the individual components. The formulation of the expected uptake for the individual components is provided subsequently. Similar trends were observed for x=1 and are reported in the supporting information (Figure S3).

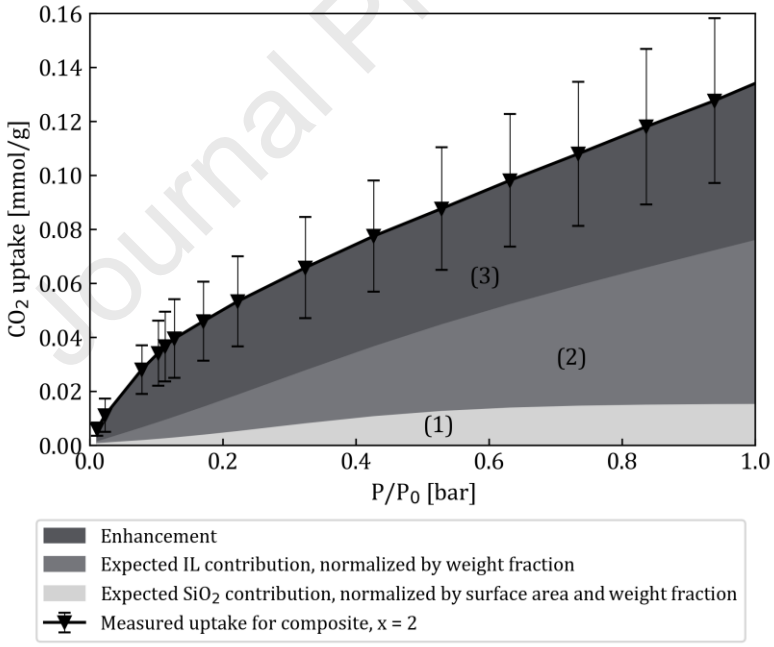

Figure 8. CO_2 uptake for the nanocomposite materials at [BMP][TFSI] to SiO_2 molar ratio x = 2 (black). The expected uptake of SiO_2 (1) is calculated as the uptake for pure SiO_2 normalized by surface area and weight fraction in the nanocomposite (0.067 (SiO_2:IL)). The expected uptake of [BMP][TFSI] is presented in (2), and calculated as the uptake for bulk ionic liquid, namely 0.0065 mmol/g for the pure ionic liquid at 0.1 bar, normalized to the ionic liquid weight fraction in the

nanocomposite [18]. The region (3) represents the uptake enhancement for the nanocomposite compared to the uptake of the individual components.

2.2.2. CO_2 UPTAKE FROM THE HOST MATRIX

In literature, the reported CO_2 uptake capacity for porous silica varies noticeably, with sometimes an order of magnitude difference between reports [22], [25]). Therefore, our mesoporous silica matrix's potential contribution of CO_2 uptake was determined experimentally. For this purpose, the ionic liquid of three of our nanocomposites (cf. supporting information S.1.3. for sample information) was removed via solvent extraction. Subsequently, the surface area of the obtained silica matrix was derived from a BET analysis of a N_2 isotherm at 77 K for these three samples (Figure S.3.). The CO_2 uptake capacity of the sol-gel SiO_2 matrix material was obtained from CO_2 isotherms at 303 K (*cf.* Experimental Methods). As expected, at a given pressure, the CO_2 uptake scaled with surface area for the three measured samples of different surface area (Figure 9a). For example, for the silica synthesized in this study, the uptake at 303 K per unit surface area was 0.1 and 0.9 mol/m^2 at 0.1 and 1 bar, respectively. Using the previously described method, a CO_2 uptake per unit surface area was determined as the linear trendline for three samples of different surface area (Figure 9b) for each partial pressure step. The obtained values are in a similar range as the CO_2 uptake for mesoporous SiO_2 reported by Mohamedali et al. and Xue et al. (0.7 mol/m^2 at 1 bar) [24], [26].

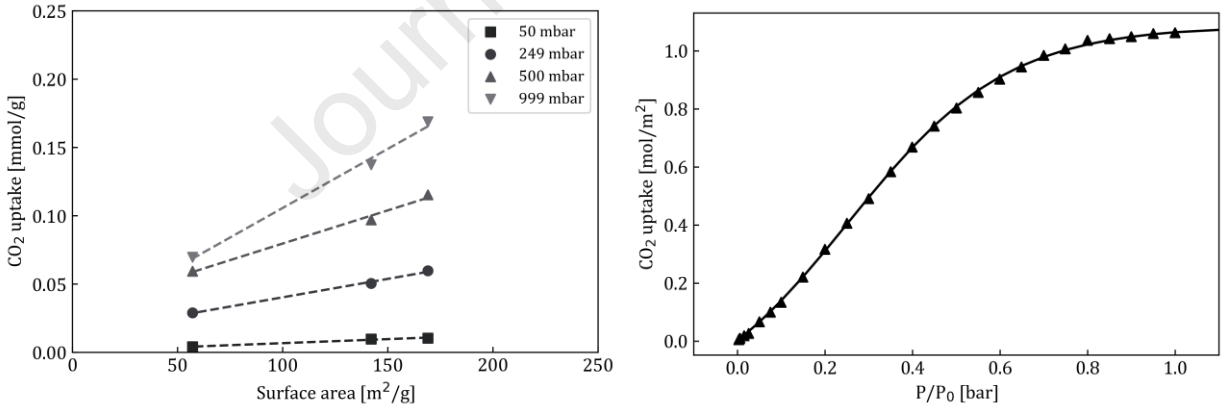

Figure 9. (a) CO_2 uptake as a function of the SiO_2 host matrix surface area after [BMP][TFSI] extraction, measured at 303K and reported at different partial pressures. The dotted lines represent the obtained trendlines of slope (■) 0.059, (•) 0.27, (▲) 0.49, (▼) 0.87 mol/m^2 that are obtained for different partial pressures. (b) CO_2 uptake normalized to SiO_2 surface area as a function of partial pressure, derived from the slopes obtained in (a) at 303 K.

A relatively high CO_2 capacity at lower partial pressures seemed to ensue from the immobilization of [BMP][TFSI] in a silica matrix (Figure 8). To quantify this increase in capacity, an "enhancement factor" (EF) was defined (Equation (3)) based on the measured uptake capacity $C_{composite}$ for the nanocomposite material, the expected ionic liquid uptake capacity C_{IL}, the IL weight fraction X_{IL}, the measured uptake capacity for SiO_2 C_{SiO2}, the host matrix surface area S and X_{SiO2} the SiO_2 weight fraction in the nanocomposite.

$$EF = \frac{\text{Measured } CO_2 \text{ uptake of the composite}}{(\text{Expected IL uptake} * \text{IL fraction}) + (\text{Expected } SiO_2 \text{ uptake} * SiO_2 \text{ fraction})}$$

$$= \frac{C_{composite}\left[\frac{mmol}{g\ composite}\right]}{C_{IL}\left[\frac{mmol}{g\ IL}\right] * X_{IL}\left[\frac{g\ IL}{g\ composite}\right] + C_{SiO_2}\left[\frac{mmol}{m^2}\right] * S\left[\frac{m^2}{g\ SiO_2}\right] * X_{SiO_2}\left[\frac{g\ SiO_2}{g\ composite}\right]} \quad (3)$$

The enhancement factor is significantly higher for composites at lower partial pressures, as can be observed in Figure 10. At partial pressures of 1 bar, the measured uptake is 1.6 to 1.7 times higher than the expected uptake from SiO_2 and the [BMP][TFSI] ionic liquid for x = 1 (black) and x = 2 (red). In this range, bulk ionic liquids are typically more performant than at low partial pressures. The possible enhancement due to interface effects is therefore expected to be less significant than at lower partial pressures as shown in Figure 8, and the enhancement factor would be expected to be closest to 1. The EF in the higher pressure range is within an order of magnitude of the heuristically expected value. The difference obtained might originate from the assumptions made and their respective variation, but overall, it supports the validity of the assumptions made for the EF model. At lower partial pressures, the enhancement factor goes up to 5 for iolnic liquid-to-silica ratios of 1 and 2. The high enhancement in uptake compared to expected values for the nanocomposites highlights the beneficial effect of ionic liquid immobilization at low partial pressures.

Interestingly, the enhancement factor remains constant regardless of x, the IL-SiO_2 molar ratio in the composite. Given that the EF for different x values considers uptake at the SiO_2 interface per surface area, interfacial effects might be the origin of the enhancement observed. In other words, when redefining the EF by taking a CO_2 uptake for SiO_2 without normalizing to surface area, a value 1.5 higher is obtained for x = 2 compared to x = 1, which matches the 1.7 times higher surface area of x = 2 compared to x = 1. Interface enhancement effects are typically correlated to ordering of the IL cation and anion pairs with the (hydrated) silanol groups on the internal silica surface. This ordering in layered structure affects the local electrostatics (electrical double layer) and chemistry (coordination). Although the notion behind interfacial effects is undisputed, the extact details of ordering of the cation, anion, CO_2, and interface groups would require highly specialized characterization and goes beyond the scope of this study. Already, for CO_2 gas sorption in bulk ionic liquids, differentiating the mechanisms behind selective uptake is not trivial, with interpretations ranging from Lewis acid-base types of interactions, changes in surface tension leading to "cavity" formation, to steric hindrance effects. Confinement of the ionic liquid into a

silica matrix adds complexity as ordering of the ionic liquid might vary depending on the chemistry used for synthesis or even the type of ionic liquid.

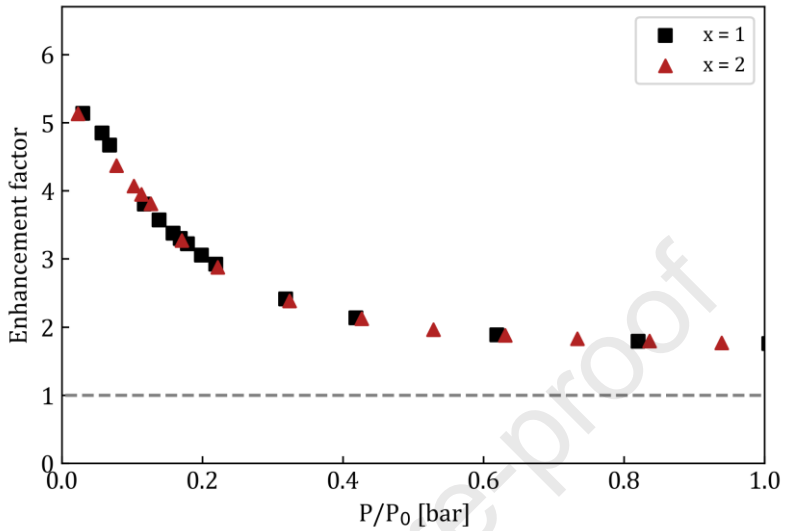

Figure 10. Enhancement factor in CO_2 uptake for nanocomposites of composition x = 1 and 2 of as a function of partial pressure. The enhancement factor is defined as the ratio between the uptake measurement for the nanocomposite divided by the expected uptake from its individual components, namely [BMP][TFSI] and SiO_2. A line is drawn for EF = 1 to guide the reader, which corresponds to an absence of enhancement.

2.3.EFFECT OF IONIC LIQUID CATION ON CO_2 UPTAKE

Next to confinement, selection of an adequate ionic liquid has been previously reported to tune uptake capacity and selectivity of the sorbent for CO_2 capture for bulk ionic liquids. Composites were synthesized with imidazolium and pyrrolidium-based ionic liquids, and the alkyl chain length of the imidazolium-based composites was varied for 2, 4 and 6 carbon atoms, while the molar ratio IL:mol SiO_2 was kept at 1. The uptake for the different composites at 0.1 bar is shown in Figure 11 and showed an increasing trend in CO_2 solubility for the respective bulk ionic liquids ([BMP][TFSI] > [HMI][TFSI] > [BMI][TFSI] > [EMI][TFSI]) [20], [46]. However, a closer look for the imidazolium-based bulk ionic liquids yields approximate CO_2 uptake capacities of 0.0069, 0.0064, 0.0068 mmol/g for [EMI][TFSI], [BMI][TFSI] and [HMI][TFSI], which would not result in the presented differences shown in Figure 11. The observed differences are therefore again most likely the result of interfacial effects. The use of bulkier cations might indeed result in a similar effect to increasing the IL-SiO_2 content, thus resulting in a higher surface area of the silica host matrix, and thereby increasing CO_2 sorption.

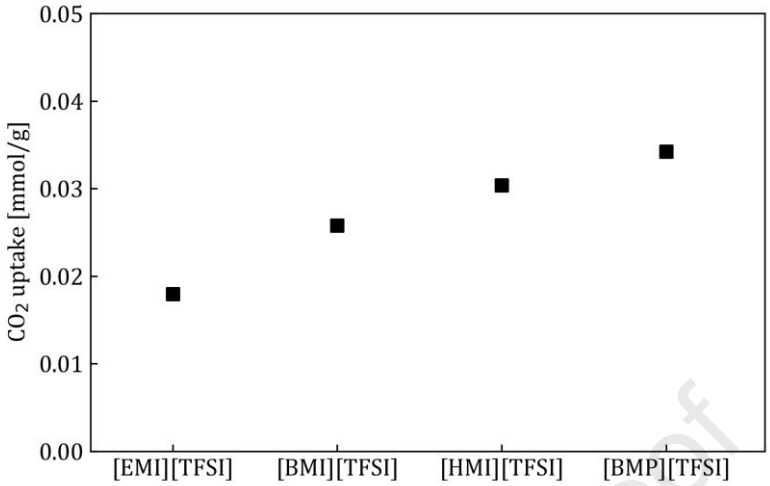

Figure 11. CO_2 uptake [mmol/g] of [$TFSI^-$]-based composites at 0.1 bar partial pressure and 303 K with imidazolium-based cations featuring increasing alkyl chain length (1-ethyl-3-methylimidazolium, 1-butyl-3-methylimidazolium and 1-hexyl-3-methylimidazolium) and for 1-butyl-1-methylpyrrolidinium, with ionic liquid-to-silica molar ratios of 1.

2.4. BENCHMARKING WITH RESPECT TO PREVIOUS REPORTS

To benchmark the performance of the synthesized materials, the enhancement factor defined in Equation (3) was computed at 0.1 bar (unless specified otherwise) for previous reports of ionic liquid-silica composites for CO_2 sorption (Table 3) at 298 K [22], 303 K [24], 313 K [23] and 323 K [26]. To compute the enhancement factors, surface area and when possible, the uptake reported for the individual components in the study were used to reduce the effect of measurement method, which are known to be considerable [13]. Though some studies showed an enhancement at a lower partial pressure of 0.1 bar, none of the latter reached enhancements as high as four, reported in our study. Interestingly, chemisorption of CO_2 for an immobilized [BMI][acetate]-silica composite was also reported in one of the studies. Computing the enhancement factor for this material, for which the sorption mechanism will differ due to the choice in ionic liquid [47], gives a much higher value of 5.8 and 4.0 on MCM-41 and SBA-15, respectively, using values reported for [BMI][acetate] [24], [48]. The enhancement in CO_2 sorption capacity at low partial pressure for the materials studied in this work appears to be in a similar range as for functionalized ionic liquid.

Table 3. Enhancement factor as defined in Equation (3), computed for previous reports of ionic liquid-silica composites for CO_2 physisorption, using the reported pure silica uptake and ionic liquid at 0.1bar and the temperature at which the study was conducted.

Ionic liquid	Enhancement factor*	Reference
[BMI][NO_3]	1.4	[22]
[BMI][$N(CN)_2$]	0.99	
[PMI][TFSI]	1.7	[24]
[PMI][TFSI]	1.5	
[EMI][TFSI]	0.45[a]	[23]
[OMI][TFSI]	0.94 [a]	
[P4444][2-Op]	2.6[b]	[26]
[BMP][TFSI]	4.1	This work, x=2

**When no report of the bulk ionic liquid uptake at the relevant pressure and temperature was found in the study, values from literature were used and are indicated by superscript [a]* [21]*. One study was reported at 0.15 bar, 50 °C, and the bulk ionic liquid uptake was extrapolated to 0.15 bar from a higher-pressure measurement assuming Henry behavior[b].*

The absolute uptake of the nanocomposites remains in a lower range compared to alternatives such as commonly studied Metal Organic Frameworks (MOF) for CO_2 capture, with *ca.* 40 times lower uptake capacity around 1 bar CO_2 and ambient temperature. To contextualize the findings, implementation of the material would be most adequate for applications requiring specific conditions, such as conformal coatings on high surface area supports. Furthermore, the enhancement insights are in general applicable to other systems.

CONCLUSION

Ionic liquid-silica composites were synthesized via a non-hydrolytic sol-gel method with a silica precursor. Using this method, high ionic liquid content composites were, for the first time, studied for CO_2 capture. In contrast to the more widely reported impregnation method, the sol-gel synthesis process offers a one-pot synthesis route without time-consuming mixing steps. Moreover, various applications can be envisioned, with possibilities for conformal thin film coatings. The confinement effect on the [$TFSI^-$] conformation was shown using Raman spectroscopy, highlighting a loss in vibrational freedom for the anion in nanocomposites with smaller average pore size and narrower pore size distribution. The interactions of the ionic liquid with its surroundings are modified upon its immobilization, which in turn impacts the material properties, such as CO_2 sorption. Overall, confinement effects of the [BMP][TFSI] in the silica matrix due to immobilization of the ionic liquid increased the uptake of the composite compared to the sum of the uptake for the two individual constituents. For composites with x = 2 mol IL: mol SiO_2, the uptake at 0.1 bar was four times higher than the expected uptake for the silica and ionic liquid

contained in the material, which is higher than enhancements found for previous studies, ranging from 0.3 to 1.4.

Confinement of sorbent materials has been shown previously to be an appealing strategy as the sorption can be increased while keeping the regeneration costs relatively low, by changing interactions between the sorbent and the sorbate [34]. Typically, physical ionic liquids are only considered promising candidates for CO_2 capture in the higher-pressure range [4]. The combination of ionic liquid and silica in the composite material enables to retain both the higher sorption capacity of silica and the selectivity of ionic liquids over other gases of interest, without having to break covalent bonds for desorption as is the case in *e.g.* chemisorption for amine-functionalized ionic liquids.

CO_2 sorption below and up to atmospheric pressure is particularly relevant in the context of the current world-wide climate mitigation policies. Strategies to enhance sorption for flue gas-like compositions, or even directed towards Direct Air Capture (DAC) are therefore needed to tackle this challenge. Despite the focus of most CO_2 sorption reports on higher pressure ranges for ionic liquid-silica composites, our research highlights possible pathways and potential strategies to enhance sorption in lower partial pressure ranges. The high ionic liquid content composites studied in this work pave the way to novel applications such as in-situ utilization of captured carbon dioxide. Poly-ionic liquids have, for example, previously been utilized as simultaneous carbon capture and utilization media [49]. The high flexibility provided by the sol-gel synthesis process enables to provide conformal coating of large surface area supports for enhanced sorption. Several alternative routes to increase CO_2 sorption can be considered to further enhance the performance of the material, for example functionalization of the silica host matrix with amine groups, or by investigating a broader range of ionic liquids with promising CO_2 uptake.

KEYWORDS
Ionogel, nanocomposite, CO_2 capture, physisorption

ACKNOWLEDGEMENTS
The authors thank Seger Witteveen his contributions to the DSC data. MvL gratefully acknowledges the support of the PhD fellowship (Grant No. 1SD5923N) from the Research Foundation Flanders (FWO) and JGD acknowledges the support of the FWO Junior Postdoctoral Fellowship (12E5123N). All the authors are grateful to VLAIO for financial support (HBC.2020.2615).

CRediT
Marieke van Leeuwen: Conceptualization, Methodology, Validation, Formal Analysis, Investigation, Writing – Original draft, Visualization, **Nina Plankensteiner**: Supervision, Validation, Project administration, Writing – Review & Editing, **Rahul Maity:** Investigation, Methodology, Writing – Review & Editing, **Jesus Gandara Loe:** Investigation, Methodology, Writing – Review & Editing, **Joeri F.M. Denayer:** Funding acquisition, Resources,

Conceptualization, Writing – Review & Editing, **Rob Ameloot:** Funding acquisition, Resources, Conceptualization, Writing – Review & Editing, **Philippe M. Vereecken:** Supervision, Validation, Funding acquisition, Resources, Conceptualization, Writing – Review & Editing.

Supporting information description (pdf)

S.1. Adsorption/desorption isotherms (.pdf)

S.1.1. CO_2 adsorption isotherms

S.1.2. Pore size distribution

S.1.3. CO_2 uptake of the silica host matrix

S.1.4. CO_2 uptake for x=1 and breakdown of expected uptake contributions

S.2. Raman spectroscopy (.pdf)

S.3. Differential Scanning Calorimetry (.pdf)

References:

[1] R. Levy and P. Przyborski, "World of Change: Global Temperature s- NASA earth observatory." Accessed: Aug. 07, 2023. [Online]. Available: https://earthobservatory.nasa.gov/world-of-change/global-temperatures

[2] "Remaining carbon budget - Mercator Research Institute on Global Commons and Climate Change (MCC)." Accessed: Feb. 02, 2022. [Online]. Available: https://www.mcc-berlin.net/en/research/co2-budget.html

[3] Intergovernmental Panel on Climate Change (IPCC), Ed., *Climate Change 2022 - Mitigation of Climate Change: Working Group III Contribution to the Sixth Assessment Report of the Intergovernmental Panel on Climate Change*. Cambridge: Cambridge University Press, 2023. doi: 10.1017/9781009157926.

[4] M. Ramdin, T. W. de Loos, and T. J. H. Vlugt, "State-of-the-Art of CO_2 Capture with Ionic Liquids," *Ind. Eng. Chem. Res.*, vol. 51, no. 24, pp. 8149–8177, Jun. 2012, doi: 10.1021/ie3003705.

[5] M. T. Ho, G. W. Allinson, and D. E. Wiley, "Reducing the Cost of CO_2 Capture from Flue Gases Using Pressure Swing Adsorption," *Ind. Eng. Chem. Res.*, vol. 47, no. 14, pp. 4883–4890, Jul. 2008, doi: 10.1021/ie070831e.

[6] G. T. Rochelle, "Amine Scrubbing for CO_2 Capture," *Science*, vol. 325, no. 5948, pp. 1652–1654, Sep. 2009, doi: 10.1126/science.1176731.

[7] L. A. Blanchard, D. Hancu, E. J. Beckman, and J. F. Brennecke, "Green processing using ionic liquids and CO_2," *Nature*, vol. 399, no. 6731, pp. 28–29, May 1999, doi: 10.1038/19887.

[8] "Dimensions," Digital Science. Accessed: Jul. 11, 2024. [Online]. Available: https://app.dimensions.ai
[9] Y. Cao and T. Mu, "Comprehensive Investigation on the Thermal Stability of 66 Ionic Liquids by Thermogravimetric Analysis," *Ind. Eng. Chem. Res.*, vol. 53, no. 20, pp. 8651–8664, May 2014, doi: 10.1021/ie5009597.
[10] X. Liu, Y. Huang, Y. Zhao, R. Gani, X. Zhang, and S. Zhang, "Ionic Liquid Design and Process Simulation for Decarbonization of Shale Gas," *Ind. Eng. Chem. Res.*, vol. 55, no. 20, pp. 5931–5944, May 2016, doi: 10.1021/acs.iecr.6b00029.
[11] S. K. Shukla, S. G. Khokarale, T. Q. Bui, and J.-P. T. Mikkola, "Ionic Liquids: Potential Materials for Carbon Dioxide Capture and Utilization," *Front. Mater.*, vol. 6, 2019, doi: 10.3389/fmats.2019.00042.
[12] J. Palomar, M. Gonzalez-Miquel, A. Polo, and F. Rodriguez, "Understanding the Physical Absorption of CO_2 in Ionic Liquids Using the COSMO-RS Method," *Ind. Eng. Chem. Res.*, vol. 50, no. 6, pp. 3452–3463, Mar. 2011, doi: 10.1021/ie101572m.
[13] P. J. Carvalho, K. A. Kurnia, and J. a. P. Coutinho, "Dispelling some myths about the CO_2 solubility in ionic liquids," *Phys. Chem. Chem. Phys.*, vol. 18, no. 22, pp. 14757–14771, Jun. 2016, doi: 10.1039/C6CP01896C.
[14] M. S. Shannon, J. M. Tedstone, S. P. O. Danielsen, M. S. Hindman, A. C. Irvin, and J. E. Bara, "Free Volume as the Basis of Gas Solubility and Selectivity in Imidazolium-Based Ionic Liquids," *Ind. Eng. Chem. Res.*, vol. 51, no. 15, pp. 5565–5576, Apr. 2012, doi: 10.1021/ie202916e.
[15] W. Shi and D. R. Luebke, "Enhanced Gas Absorption in the Ionic Liquid 1-n-Hexyl-3-methylimidazolium Bis(trifluoromethylsulfonyl)amide ([hmim][Tf2N]) Confined in Silica Slit Pores: A Molecular Simulation Study," *Langmuir*, vol. 29, no. 18, pp. 5563–5572, May 2013, doi: 10.1021/la400226g.
[16] J. Zhang *et al.*, "Nanocomposites of ionic liquids confined in mesoporous silica gels: preparation, characterization and performance," *Phys. Chem. Chem. Phys.*, vol. 12, no. 8, pp. 1971–1981, 2010, doi: 10.1039/B920556J.
[17] L. A. Banu, D. Wang, and R. E. Baltus, "Effect of Ionic Liquid Confinement on Gas Separation Characteristics," *Energy Fuels*, vol. 27, no. 8, pp. 4161–4166, Aug. 2013, doi: 10.1021/ef302038e.
[18] J. Kumełan, D. Tuma, Á. Pérez-Salado Kamps, and G. Maurer, "Solubility of the Single Gases Carbon Dioxide and Hydrogen in the Ionic Liquid [bmpy][Tf2N]," *J. Chem. Eng. Data*, vol. 55, no. 1, pp. 165–172, Jan. 2010, doi: 10.1021/je900298e.
[19] E. Privalova, P. Mäki-Arvela, D. Murzin, and J. Mikkhola, "Capturing CO_2: Conventional versus ionic-liquid based technologies," *Russ. Chem. Rev. - RUSS CHEM REV-ENGL TR*, vol. 81, pp. 435–457, May 2012, doi: 10.1070/RC2012v081n05ABEH004288.
[20] J. L. Anderson, J. K. Dixon, and J. F. Brennecke, "Solubility of CO_2 , CH_4 , C_2H_6 , C_2H_4 , O_2 , and N_2 in 1-Hexyl-3-methylpyridinium Bis(trifluoromethylsulfonyl)imide: Comparison to Other Ionic Liquids," *Acc. Chem. Res.*, vol. 40, no. 11, pp. 1208–1216, Nov. 2007, doi: 10.1021/ar7001649.
[21] Y. S. Sistla and A. Khanna, "Validation and Prediction of the Temperature-Dependent Henry's Constant for CO_2–Ionic Liquid Systems Using the Conductor-like Screening Model for Realistic Solvation (COSMO-RS)," *J. Chem. Eng. Data*, vol. 56, no. 11, pp. 4045–4060, Nov. 2011, doi: 10.1021/je200486c.

[22] M. Mirzaei, A. R. Badiei, B. Mokhtarani, and A. Sharifi, "Experimental study on CO_2 sorption capacity of the neat and porous silica supported ionic liquids and the effect of water content of flue gas," *J. Mol. Liq.*, vol. 232, pp. 462–470, Apr. 2017, doi: 10.1016/j.molliq.2017.02.104.

[23] J. Zhu, B. He, J. Huang, C. Li, and T. Ren, "Effect of immobilization methods and the pore structure on CO_2 separation performance in silica-supported ionic liquids," *Microporous Mesoporous Mater.*, vol. 260, pp. 190–200, Apr. 2018, doi: 10.1016/j.micromeso.2017.10.035.

[24] M. Mohamedali, H. Ibrahim, and A. Henni, "Imidazolium based ionic liquids confined into mesoporous silica MCM-41 and SBA-15 for carbon dioxide capture," *Microporous Mesoporous Mater.*, vol. 294, p. 109916, Mar. 2020, doi: 10.1016/j.micromeso.2019.109916.

[25] B. B. Polesso, R. Duczinski, F. L. Bernard, and H. Z. Ferrari, "Imidazolium-based Ionic Liquids Impregnated in Silica and Alumina Supports for CO_2 Capture," *Mater. Res.*.

[26] C. Xue *et al.*, "Pyridine-containing ionic liquids lowly loaded in large mesoporous silica and their rapid CO_2 gas adsorption at low partial pressure," *J. CO_2 Util.*, vol. 34, pp. 282–292, Dec. 2019, doi: 10.1016/j.jcou.2019.06.015.

[27] C. Xue *et al.*, "High and fast carbon dioxide capture of hydroxypyridine-based ionogel depending on pore structure of mesoporous silica vesicle in the simulated flue gas," *Int. J. Greenh. Gas Control*, vol. 84, pp. 111–120, May 2019, doi: 10.1016/j.ijggc.2019.03.017.

[28] H. Kolding, R. Fehrmann, and A. Riisager, "CO_2 Capture technologies: Current status and new directions using supported ionic liquid phase (SILP) absorbers," *Sci. China Chem.*, no. 55, p. 1648, 2012.

[29] J. Aboudi and M. Vafaeezadeh, "Efficient and reversible CO_2 capture by amine functionalized-silica gel confined task-specific ionic liquid system," *J. Adv. Res.*, vol. 6, no. 4, pp. 571–577, Jul. 2015, doi: 10.1016/j.jare.2014.02.001.

[30] G. Em. Romanos *et al.*, "CO_2 Capture by Novel Supported Ionic Liquid Phase Systems Consisting of Silica Nanoparticles Encapsulating Amine-Functionalized Ionic Liquids," *J. Phys. Chem. C*, vol. 118, no. 42, pp. 24437–24451, Oct. 2014, doi: 10.1021/jp5062946.

[31] M. I. Onishchenko, I. A. Tyablikov, E. E. Knyazeva, V. V. Chernyshev, A. V. Yatsenko, and B. V. Romanovsky, "Modification of MCM-41 and SBA-15 mesoporous silicas by imidazolium ionic liquids," *Russ. J. Phys. Chem. A*, vol. 87, no. 1, pp. 108–113, Jan. 2013, doi: 10.1134/S0036024413010159.

[32] R. Maity *et al.*, "Strategic Fast Induction Heating to Combat Hysteresis Barriers in a Flexible MOF for Rapid CO_2 Desorption in Biogas Upgrading," *Small*, vol. 19, no. 29, p. 2302893, 2023, doi: 10.1002/smll.202302893.

[33] M. Nagendrachar Garaga, L. Aguilera, N. Yaghini, A. Matic, M. Persson, and A. Martinelli, "Achieving enhanced ionic mobility in nanoporous silica by controlled surface interactions," *Phys. Chem. Chem. Phys.*, vol. 19, no. 8, pp. 5727–5736, 2017, doi: 10.1039/C6CP07351D.

[34] X. Ma, X. Wang, and C. Song, "'Molecular Basket' Sorbents for Separation of CO_2 and H_2S from Various Gas Streams," *J. Am. Chem. Soc.*, vol. 131, no. 16, pp. 5777–5783, Apr. 2009, doi: 10.1021/ja8074105.

[35] X. Chen and P. M. Vereecken, "Solid and Solid-Like Composite Electrolyte for Lithium Ion Batteries: Engineering the Ion Conductivity at Interfaces," *Adv. Mater. Interfaces*, vol. 6, no. 1, p. 1800899, 2019, doi: 10.1002/admi.201800899.

[36] O. V. Mazurin, M. V. Streltsina, and T. P. Shvaiko-Shvaikovskaya, *Handbook of glass data. Part A. silica glass and binary silicate glasses*. Elsevier Science Publishers B.V., 1983.
[37] T. Liu, Y. Danten, J. Grondin, and R. Vilar, "Solvation of AgTFSI in 1-ethyl-3-methylimidazolium bis(trifluoromethylsulfonyl)imide ionic liquid investigated by vibrational spectroscopy and DFT calculations," *J. Raman Spectrosc.*, vol. 47, no. 4, pp. 449–456, 2016, doi: 10.1002/jrs.4835.
[38] M. Herstedt *et al.*, "Spectroscopic characterization of the conformational states of the bis(trifluoromethanesulfonyl)imide anion ($TFSI^-$)," *J. Raman Spectrosc.*, vol. 36, no. 8, pp. 762–770, 2005, doi: 10.1002/jrs.1347.
[39] T. Watkins and D. A. Buttry, "Determination of Mg^{2+} Speciation in a $TFSI^-$-Based Ionic Liquid With and Without Chelating Ethers Using Raman Spectroscopy," *J. Phys. Chem. B*, vol. 119, no. 23, pp. 7003–7014, Jun. 2015, doi: 10.1021/acs.jpcb.5b00339.
[40] J.-C. Lassègues, J. Grondin, and D. Talaga, "Lithium solvation in bis(trifluoromethanesulfonyl)imide-based ionic liquids," *Phys. Chem. Chem. Phys.*, vol. 8, no. 48, pp. 5629–5632, Dec. 2006, doi: 10.1039/B615127B.
[41] M. Herstedt *et al.*, "Conformational isomerism and phase transitions in tetraethylammonium bis(trifluoromethanesulfonyl)imide Et4NTFSI," *J. Mol. Struct.*, vol. 783, no. 1, pp. 145–156, Feb. 2006, doi: 10.1016/j.molstruc.2005.08.028.
[42] T. Liu, "Electrodéposition de couches minces métalliques à partir de solutions de liquides ioniques pour des applications électroniques.," phdthesis, Université de Bordeaux ; Universidade nova de Lisboa. Faculdade de ciências e tecnologia (Lisboa, Portugal), 2014. Accessed: Aug. 19, 2024. [Online]. Available: https://theses.hal.science/tel-01142699
[43] Y. Umebayashi *et al.*, "Lithium Ion Solvation in Room-Temperature Ionic Liquids Involving Bis(trifluoromethanesulfonyl) Imide Anion Studied by Raman Spectroscopy and DFT Calculations," *J. Phys. Chem. B*, vol. 111, no. 45, pp. 13028–13032, Nov. 2007, doi: 10.1021/jp076869m.
[44] A. Marie *et al.*, "Silica based ionogels: interface effects with aprotic and protic ionic liquids with lithium," *Phys. Chem. Chem. Phys.*, vol. 22, no. 41, pp. 24051–24058, Oct. 2020, doi: 10.1039/D0CP03599H.
[45] A. Sagara *et al.*, "Interfacial Conductivity Enhancement and Pore Confinement Conductivity-Lowering Behavior inside the Nanopores of Solid Silica-gel Nanocomposite Electrolytes," *ACS Appl. Mater. Interfaces*, vol. 13, no. 34, pp. 40543–40551, Sep. 2021, doi: 10.1021/acsami.1c09246.
[46] J. L. Anthony, J. L. Anderson, E. J. Maginn, and J. F. Brennecke, "Anion Effects on Gas Solubility in Ionic Liquids," *J. Phys. Chem. B*, vol. 109, no. 13, pp. 6366–6374, Apr. 2005, doi: 10.1021/jp046404l.
[47] P. V. Kortunov, L. S. Baugh, and M. Siskin, "Pathways of the Chemical Reaction of Carbon Dioxide with Ionic Liquids and Amines in Ionic Liquid Solution," *Energy Fuels*, vol. 29, no. 9, pp. 5990–6007, Sep. 2015, doi: 10.1021/acs.energyfuels.5b00876.
[48] E. J. Maginn, "Design and evaluation of ionic liquids as novel CO_2 absorbents," University of Notre Dame (US), Dec. 2004. doi: 10.2172/836826.
[49] T. Benedetti, S. Naficy, A. Walker, D. L. Officer, G. G. Wallace, and F. Dehghani, "Solid-State Poly(ionic liquid) Gels for Simultaneous CO_2 Adsorption and Electrochemical Reduction," *Energy Technol.*, vol. 6, no. 4, pp. 702–709, 2018, doi: 10.1002/ente.201700679.

Table of contents:

Highlights

"Surface enhanced CO_2 capture in ionic liquid-silica nanocomposites via sol-gel synthesis in the low partial pressure range"

- 14 times higher ionic liquid to silica weight ratio than state-of-the-art
- Enhanced CO_2 sorption at low P_{CO2}
- Sol-gel method enables more versatile applications (e.g. conformal coatings)

Declaration of interests

☒ The authors declare that they have no known competing financial interests or personal relationships that could have appeared to influence the work reported in this paper.

☐ The authors declare the following financial interests/personal relationships which may be considered as potential competing interests: